Supplementary Material:
Escalating environmental summer heat exposure – a future threat for the European workforce

Ana Casanueva[1,2], Sven Kotlarski[1], Andreas M. Fischer[1], Andreas D. Flouris[3], Tord Kjellstrom[4,5], Bruno Lemke[6], Lars Nybo[7], Cornelia Schwierz[1] and Mark A. Liniger[1]

[1]Federal Office of Meteorology and Climatology MeteoSwiss, Zurich, Switzerland
[2]Meteorology Group, Dept. Applied Mathematics and Computer Science, University of Cantabria, Santander, Spain
[3]FAME Laboratory, Department of Exercise Science, University of Thessaly, Karies, Trikala, Greece
[4]Centre for Technological Research and Innovation (CETRI), Limmasol, Cyprus
[5]Australian National University, Canberra, Australia
[6]Nelson-Marlborough Institute of Technology, Nelson, New Zealand
[7] Department of Nutrition and Exercise Sciences, University of Copenhagen, Copenhagen, Denmark

Corresponding author: ana.casanueva@unican.es

Annex A: Sensitivity of WBGT to daily aggregated input parameters

Heat stress and its consequences occur at high temporal (e.g. hourly) and spatial (individual person) level. However, very often climate data from observations and models (including the EURO-CORDEX RCMs considered) do not provide public sub-daily data. To circumvent the lack of data at hourly resolution, we focus on the daily maximum heat exposure, i.e. the maximum value of a given heat index throughout the course of a day, in order to target the most extreme situations. For this purpose, we need to find the best approximation for the maximum daily heat index value based on daily aggregated input parameters. $WBGT_{shade}$ depends only on temperature and dew point. Assuming that dew point temperature does not vary much during the day, the maximum $WBGT_{shade}$ could be approximated with daily maximum temperature and daily mean dew point temperature, which are variables available from the model data and observations. $WBGT_{sun}$ depends also on wind speed and solar radiation. Additionally, the hour of the day is relevant for the zenith angle calculation that modifies the contribution of the solar radiation and, thus, the calculated $WBGT_{sun}$. We tested different combinations of daily aggregated parameters that could potentially approximate the maximum daily WBGT obtained from hourly data. For this purpose, we consider hourly data from SMN observations and analyze some representative stations in Switzerland (Figure S1). The considered approximations (Y-axes in the Q-Q plots) are: daily mean values for all parameters and time of day set to 15h (blue), daily mean values for all parameters and time of day set to 12h (green), daily maximum temperature and mean values for the rest of the parameters and time of day set to 12h (magenta), daily maximum temperature and mean values for the rest of the parameters and time of day set to 15h (red) and daily maximum temperature and radiation and mean values for the rest of the parameters and time of day set to 12h (black). We find a clear underestimation of $WBGT_{sun}$ when daily mean temperature is used, whereas the time of the day has a very small impact on the result (blue and green). The use of daily maximum temperature (magenta and red) clearly improves the situation, being the quantiles closer to the diagonal. However, there is still some underestimation of approximately 2°C with respect to the real daily maximum $WBGT_{sun}$. The best approximation is obtained using daily maximum values of temperature and solar radiation (black). From these results, we conclude that we can reliably estimate the daily maximum $WBGT_{sun}$ using daily maximum temperature and radiation and daily mean values of dew point temperature and wind speed.

Annex B: Comparison of derived heat exposure indices

Several derived indices (e.g. mean, maximum and frequencies of threshold exceedances) have been calculated from the daily maximum values of WBGT (Table 1). Note that monthly mean values based on daily maximum WBGT are about 3°C higher than the mean of 24-hour WBGT values (not shown). Additionally, different temporal aggregations (seasons, months) to summarize information should be carefully interpreted. For instance, monthly means in June are around 1-2°C lower than July and August in much of Europe (Table S1), which means that the seasonal (JJA) mean values will underestimate the peak heat exposure periods. The peak values for 1-day (WBGTx1d) and 3-day moving average (WBGTx3d) periods compared to monthly mean of WBGT are considerably higher in the two exemplary cooler cities, which indicates the role of heat waves in bringing up exceptional heat among coolest days due to the effect of wind. In Lugano, Rome and Seville, WBGTx3d (WBGTx1d) is approximately 3.5-4°C (4.5-5°C) higher than the summer mean (Table S1). For the sake of conciseness all analyses are carried out at a seasonal level (i.e. JJA maximum for each year regardless of the month when it occurs). To increase robustness in the transient results in Fig.1, the summer maximum for each year was taken from a smoothed series using a 3-day moving average (WBGTx3d). The comparison of both quantities (single-day maximum and maximum of moving 3-day average WBGT) is given in Table S1. The frequency of situations with moderate and high risk of heat stress is determined by calculating the number of days above certain thresholds (26°C and 28° as exposure limits for unacclimatized and acclimatized individuals, respectively, for moderate work intensity (300-350W), WBGTg26 and WBGTg28). In all cases the indices are calculated for each summer and the mean over 30 years is taken as the final value.

Annex C: Sources of uncertainty and limitations

Relating climate change and productivity losses is not a simple matter and there is a number of assumptions and limitations that need to be considered. Some of the main limitations and sources of uncertainty are included hereunder:

- **Observational uncertainty.** Different sources of observational data were merged to provide a dense enough network of stations in Europe. Detailed analyses were performed to check 1) the quality of the GSOD data set for locations where ECA and GSOD are available, and 2) the accuracy of using radiation data from satellite instead of ground observations (not shown). For (1) both datasets were compared for the set common stations (located in Spain, Germany, Norway, Netherlands and Slovakia) in the two datasets. Although there are some differences at the daily scale, the main characteristics of the distribution and ranks (which are later on used in the quantile mapping approach) are very consistent. For (2) the satellite data (5x5km grid) were compared with ground observations available at the SwissMetNet stations. Although there are some statistically significant differences in the solar radiation distribution, the null hypothesis of similarity of distributions cannot be rejected for WBGT at a significance level of 0.01, probably due to the lower sensitivity of WBGT to small changes in radiation (Fig. S4).
- **Climate model and scenario uncertainty.** It is essential to use a large enough ensemble of models to produce robust climate change projections. In most of the results, the multi-model median is used for the sake of brevity, but the robustness of these signals is analyzed in the section "Model uncertainty in the climate change signal". Emission scenario uncertainty is included throughout the manuscript covering low, medium and strong emission scenarios.
- **WBGT as heat exposure index.** WBGT consists of the combination of several meteorological variables, thus it represents heat exposure. One index for general environmental warning at population level may be too simple to cover all scenarios and more sophisticated and complex indices should be used for evaluating specific work conditions when individual factors such as clothing, metabolic heat production, age, gender and acclimatization state are known. Those complex thermophysiological models are undergoing significant development and advancements, however their acceptance still seems limited and confined to research (Havenith and Fiala, 2015). In the present study we establish the environmental basis at a European scale for subsequent and more specific, individual-dependent analyses.

- **<u>Effect of model biases and observational errors on the WBGT.</u>** We acknowledge that some of the input variables of the WBGT in the sun have not been broadly evaluated in the models and their quality in the observations is subject to discussion (e.g. wind speed). Response surfaces were analyzed to give an insight into the sensitivity of WBGT to changes in the input variables. Small changes in wind and radiation coming from potential observational uncertainties or remaining biases are only of minor relevance for the WBGT, whereas air temperature and dew point temperature play a major role (Fig.S4).
- **<u>Bias correction method.</u>** Quantile mapping is one of the best performing bias correction and downscaling methods in intercomparison studies (Gudmundsson, et al., 2012; Gutiérrez, et al., 2018; Hertig, et al., 2018) and is a good candidate in a multi-variate context since the inter-variable consistency is largely preserved after the independent correction of the parameters (Wilcke, et al., 2013). It is, however, subject to a number of limitations and shortcomings (Maraun, et al., 2017; Lanzante, et al., 2018): it is assumed that biases remain stationary in time (stationarity assumption) which is debatable under climate change conditions (Ehret, et al., 2012); biases are not related to the (mis)representation of physical processes in the models such as synoptic circulation (Addor, et al., 2016); changes in trends or spatio-temporal structures that may appear due to the scale mismatch between model and observations when it is used as downscaling method (Maraun, 2013); debatable deviations from the raw model signal may appear as a consequence of the treatment of “new extremes” (Gobiet, et al., 2015; Casanueva, et al., 2018; Ivanov, et al., 2018); inter-variable dependencies might be modified to some extent (Ehret, et al., 2012; Vrac and Friederichs, 2015). To account for the remaining uncertainty at the upper edge of the WBGT distribution coming from the constant extrapolation applied to “new extremes” (Ivanov, et al., 2018) we performed an additional split sample cross-validation (cold vs. warm years, not shown). This indicated that the effect on WBGT extremes is small and of the same order of magnitude as in the non-cross-validated analysis (Fig. S5).
- **<u>Losses in productivity.</u>** Due to the lack of freely accessible subdaily observational and model data an approximation is used to disaggregate daily into subdaily values (Kjellstrom, et al., 2018). Exposure-response curves relating heat stress and productivity might substantially vary from the ISO standards (ISO, 1989) to epidemiological studies (Wyndham, 1969; Sahu, et al., 2013), and would further depend on the industrial sector of interest and the individual features. As a compromise, we use the international standards, which would be more restrictive than epidemiological studies because they are based on heat levels that protect most of the workforce.

- **Urban heat island effect.** Climate simulations using urban models show that heat stress is higher in urban areas compared to neighboring rural areas (Fischer, et al., 2012). This effect is not considered in the present work since the EURO-CORDEX simulations do not include dedicated urban modules and most of the meteorological stations are located in the city outskirts. Therefore, our results might underestimate heat exposure in the centers of European cities.

Annex D: Supplementary Tables

Table S1 Comparison of derived heat indices. Observed indices in 5 European cities for WBGT in the shade and in the sun (°C) for the period 1981-2010: 30-year mean of the daily maximum values (WBGTmean), 30-year mean of the highest WBGT per month and season (WBGTx1day) and 30-year mean of the highest WBGT per month and season from the smoothed series with a 3-day moving average (WBGTx3d). All calculations are obtained for each month and the entire summer season (JJA) and based on daily maximum values of WBGT (see Annex B "Comparison of derived heat stress indices").

		Shade			**Sun**		
Location	**Month**	**WBGTmean**	**WBGTx1d**	**WBGTx3d**	**WBGTmean**	**WBGTx1d**	**WBGTx3d**
Oslo (NO)	June	15.35	20.49	19.41	17.94	23.52	22.35
	July	17.66	21.97	21.24	20.18	25.05	24.18
	August	16.72	20.89	20.11	19.15	23.94	22.96
	JJA	16.59	22.57	21.81	19.1	25.62	24.8
Berlin (DE)	June	17.29	23.73	22.36	19.64	26.35	25.09
	July	19.5	24.96	23.74	21.86	27.79	26.53
	August	19.2	24.63	23.34	21.64	27.42	26.12
	JJA	18.68	26.07	24.58	21.06	28.79	27.38
Lugano (CH)	June	19.65	23.7	23.22	22.76	27.13	26.64
	July	21.86	25.02	24.49	25.08	28.46	27.94
	August	21.46	24.52	24.14	24.6	28	27.54
	JJA	21	25.43	24.92	24.16	28.87	28.34
Rome (IT)	June	22.57	26.15	25.6	25.62	29.34	28.72
	July	25.22	27.96	27.44	28.21	31.07	30.49
	August	25.56	28.54	27.92	28.55	31.46	30.89
	JJA	24.49	28.9	28.19	27.51	31.86	31.19
Seville (SP)	June	24.38	28.23	27.6	27.07	30.99	30.38
	July	26.89	30.29	29.55	29.68	32.95	32.35
	August	26.95	30.32	29.48	29.76	33.03	32.31
	JJA	26.09	30.81	29.87	28.86	33.41	32.66

Table S2 GCM-RCM simulations. Summary of the EURO-CORDEX simulations considered in the present work. Subscripts “h” and “w” indicate that daily mean relative humidity and wind speed were not available for these specific simulations, thus they were derived from the daily values of the available parameters.

			RCP2.6		RCP4.5		RCP8.5	
RCM	**GCM**	**Member**	**EUR-11**	**EUR-44**	**EUR-11**	**EUR-44**	**EUR-11**	**EUR-44**
CLMcom-CCLM4-8-17	CNRM-CERFACS-CNRM-CM5	r1i1p1			X^h		X^h	
CLMcom-CCLM4-8-17	ICHEC-EC-EARTH	r12i1p1			X^h		X^h	
CLMcom-CCLM4-8-17	MOHC-HadGEM2-ES	r1i1p1			X^h		X^h	X
CLMcom-CCLM4-8-17	MPI-M-MPI-ESM-LR	r1i1p1			X^h	X^h	X^h	X^h
CLMcom-CCLM5-0-6	CNRM-CERFACS-CNRM-CM5	r1i1p1						X
CLMcom-CCLM5-0-6	ICHEC-EC-EARTH	r12i1p1						X
CLMcom-CCLM5-0-6	MIROC-MIROC5	r1i1p1						X
CLMcom-CCLM5-0-6	MOHC-HadGEM2-ES	r1i1p1						X
CLMcom-CCLM5-0-6	MPI-M-MPI-ESM-LR	r1i1p1						X
CNRM-ALADIN53	CNRM-CERFACS-CNRM-CM5	r1i1p1			X^w	X^w	X^w	X^w
DMI-HIRHAM5	ICHEC-EC-EARTH	r3i1p1	X		X	X	X	X
HMS-ALADIN52	CNRM-CERFACS-CNRM-CM5	r1i1p1						X
KNMI-RACMO22E	ICHEC-EC-EARTH	r1i1p1			X	X	X	X
KNMI-RACMO22E	MOHC-HadGEM2-ES	r1i1p1	X	X	X	X	X	X
MPI-CSC-REMO2009	MPI-M-MPI-ESM-LR	r1i1p1	X^h	X^h	X^h	X^h	X^h	X^h
MPI-CSC-REMO2009	MPI-M-MPI-ESM-LR	r2i1p1	X^h	X^h	X^h	X^h	X^h	X^h
SMHI-RCA4	CCCma-CanESM2	r1i1p1				X		X
SMHI-RCA4	CNRM-CERFACS-CNRM-CM5	r1i1p1			X	X	X	X
SMHI-RCA4	CSIRO-QCCCE-CSIRO-Mk3-6-0	r1i1p1				X		X
SMHI-RCA4	ICHEC-EC-EARTH	r12i1p1	X	X	X	X	X	X
SMHI-RCA4	IPSL-IPSL-CM5A-MR	r1i1p1			X	X	X	X
SMHI-RCA4	MIROC-MIROC5	r1i1p1		X		X		X
SMHI-RCA4	MOHC-HadGEM2-ES	r1i1p1		X	X	X	X	X
SMHI-RCA4	MPI-M-MPI-ESM-LR	r1i1p1		X	X	X	X	X
SMHI-RCA4	NCC-NorESM1-M	r1i1p1		X		X		X
SMHI-RCA4	NOAA-GFDL-GFDL-ESM2M	r1i1p1				X		X
TOTAL			**5**	**8**	**15**	**17**	**15**	**24**
TOTAL PER SCENARIO			**13**		**32**		**39**	

Annex E: Supplementary Figures

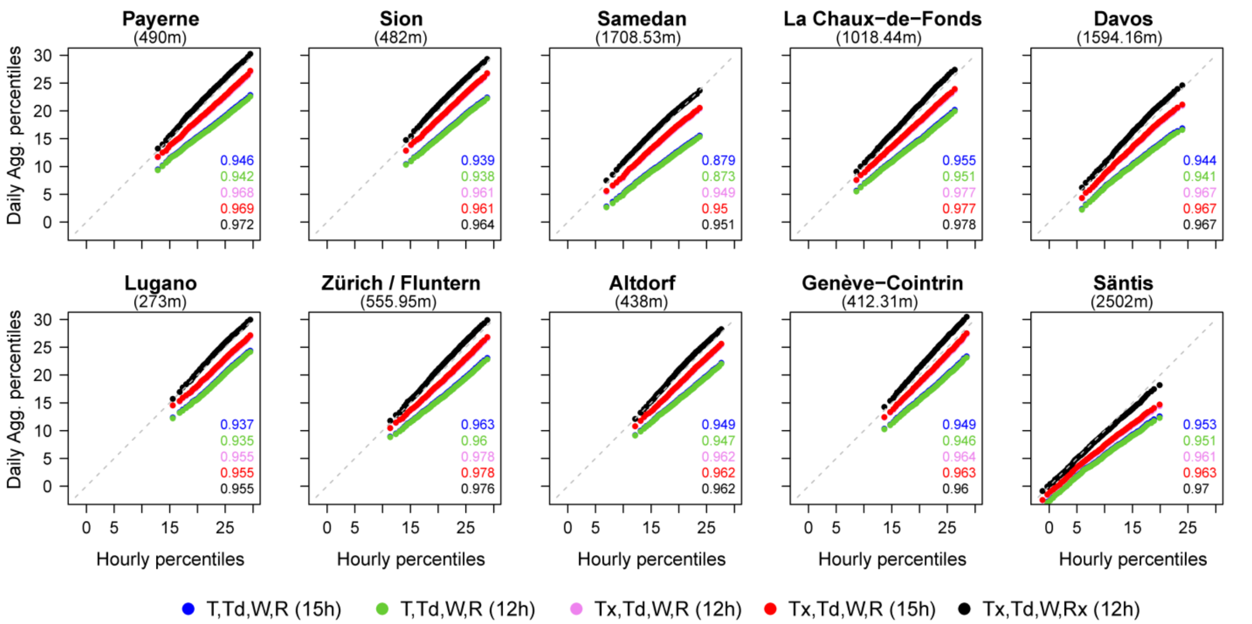

Figure S1 Sensitivity of WBGT to daily aggregated input parameters. Q-Q plots showing the 99 percentiles of summer daily maximum $WBGT_{sun}$ obtained from hourly data (X-axis) vs. $WBGT_{sun}$ calculated from different daily aggregated values (Y-axis), for 10 representative stations in Switzerland (altitude in brackets), where sub-daily data are available for the comparison. Subscript "x" refers to daily maximum parameter, otherwise daily mean in used. Spearman correlation values between the pairs of series are provided in each case (colored numbers).

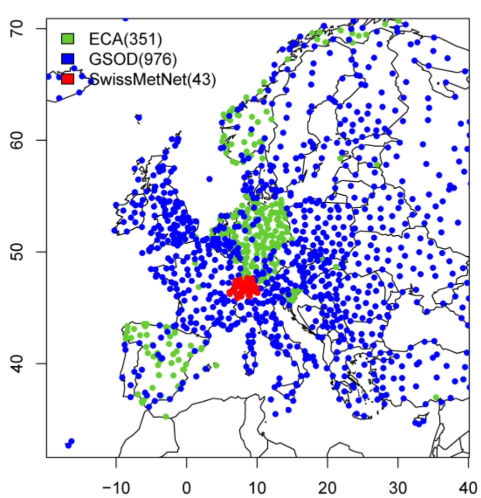

Figure S2 Observational datasets. European stations considered in this work, from ECA&D (green), GSOD (blue) and SMN (red).

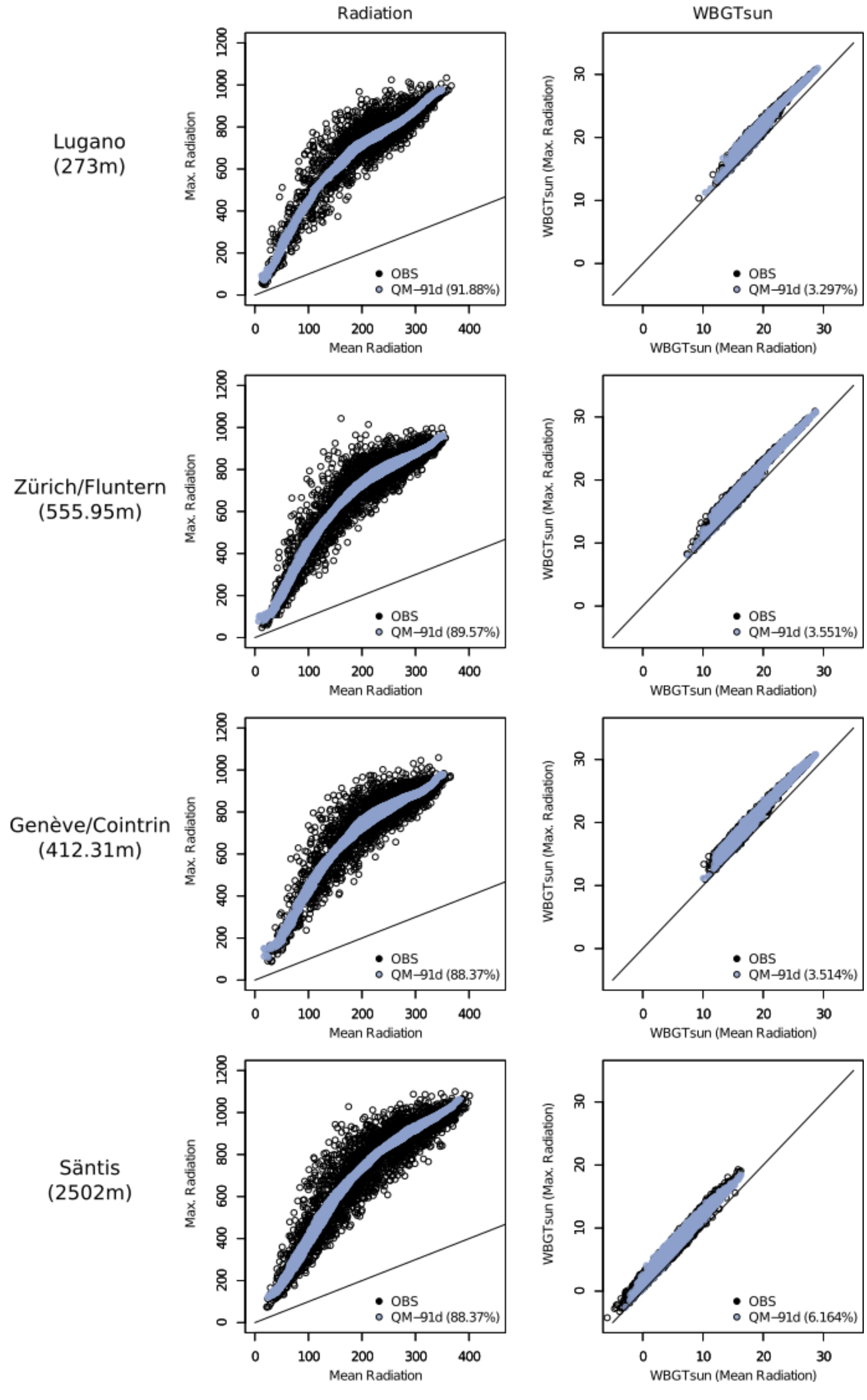

Figure S3 Test of the application of quantile mapping (QM-91d) to bias-correct daily mean solar radiation from the model against daily maximum observed solar radiation. The scatter plots show pairs of summer values of daily mean radiation (X-axis) against daily maximum radiation (Y-axis) as represented by the observations (black) and after QM (blue; model: KNMI-RACMO-HADGEM-EUR11), for the historical period 1981-2010 and four representative stations in Switzerland (left column). The percentages in the legend depict the amount of data outside the observed range. Note that QM of daily mean radiation against daily maximum values leads to a large reduction of variability compared to the observed range, since with QM one value is always corrected with the correction function from the corresponding percentile, regardless of subdaily characteristics, cloudiness, etc. The right panel represents $WBGT_{sun}$ when either daily mean (X-axis) or daily maximum (Y-axis) radiation are used in the calculation, for the observations (black) and bias-corrected model (blue). Most of the variability of WBGT is relatively well captured, even in locations with complex orography.

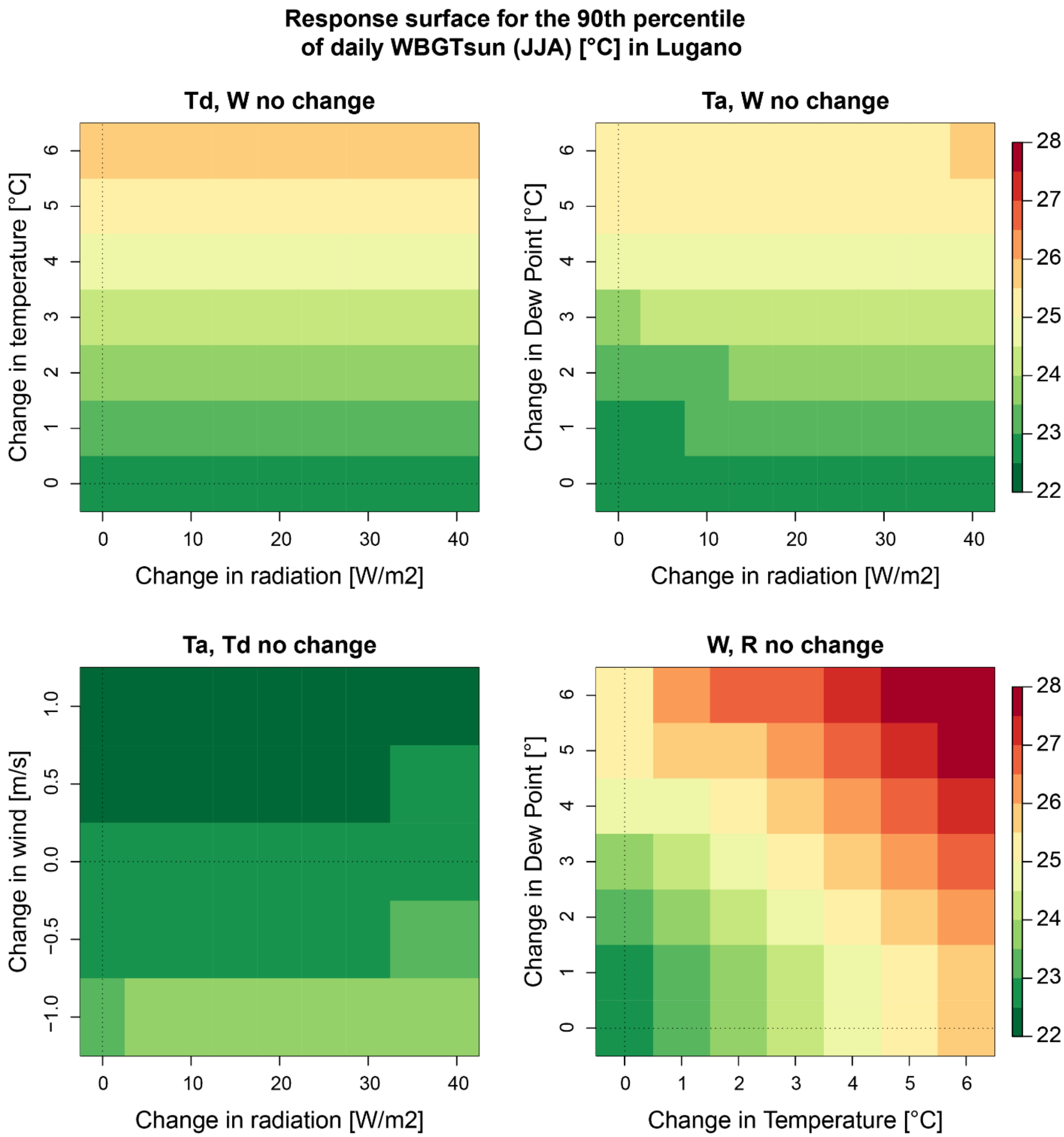

Figure S4 Response surfaces for the 90th percentile of $WBGT_{sun}$ for Lugano (Switzerland) in summer. Example for Lugano of the sensitivity of WBGT to changes in the input variables. The intersection of the dashed lines in each panel represents the mean value in present-day climate, and the colors represent values of the 90th percentile of $WBGT_{sun}$ when pairs of input variables are increased or decreased (X- and Y-axis), keeping the other two variables constant. T_a: air temperature, T_d: dew point temperature, W: wind speed, R: solar radiation.

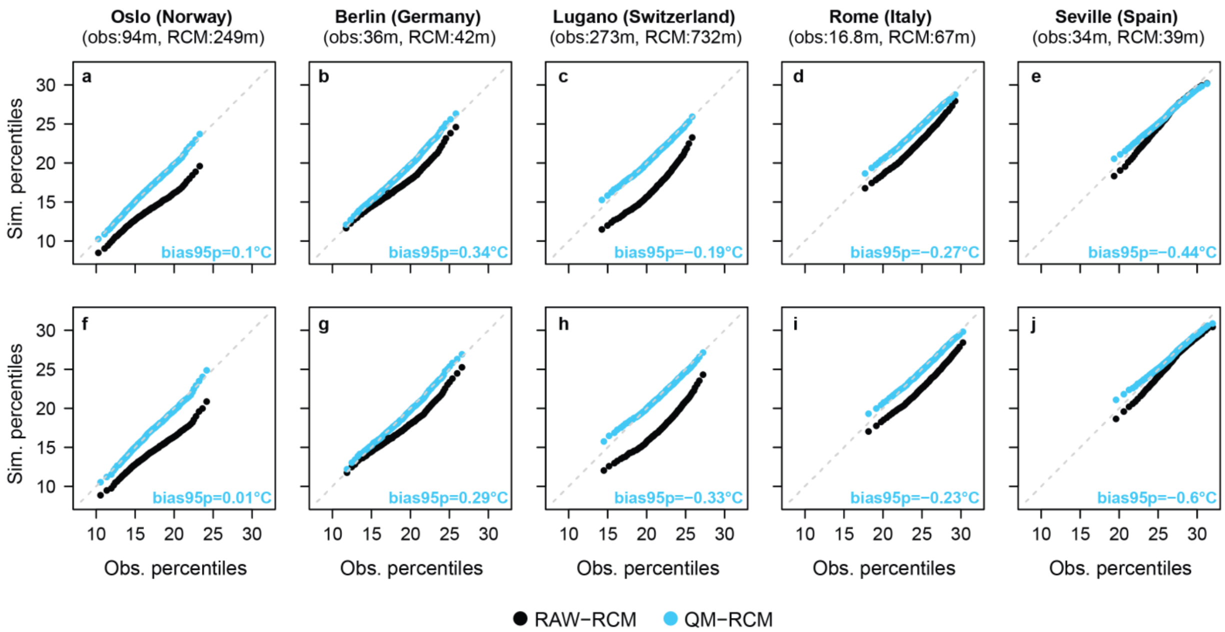

Figure S5 Evaluation of the quantile mapping in the multivariate context. Q-Q plots for the observed vs. simulated quantiles of summer $WBGT_{shade}$ (a-e) and $WBGT_{sun}$ (f-j) for five representative stations in Europe for the period 1981-2010. The black (blue) dots represent the quantiles for the raw (bias-corrected) data. This is an example for a single model chain (CLMCOM-CCLM4-MPIESM-EUR11). The real altitude of the stations and the corresponding one in the closest RCM grid box are given in brackets. Biases of the 95th percentile of the bias-corrected WBGT are given in each plot.

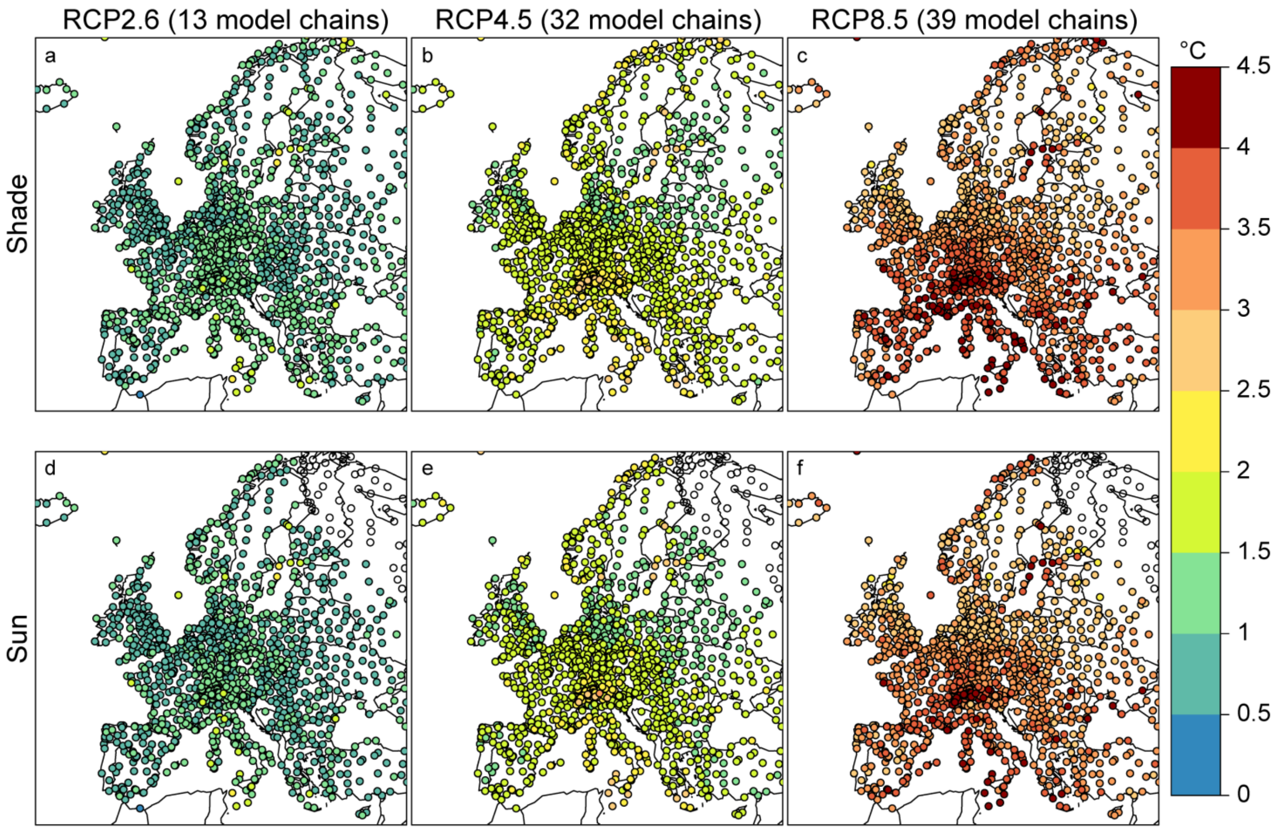

Figure S6 Climate change signal of summer maximum heat exposure. Climate change signal for summer maximum WBGT (WBGTx1day) in the shade (a-c) and in the sun (d-f) for the three RCPs (columns) for the period 2070-2099 with respect to 1981-2010. Each map represents the multi-model ensemble median, the number of model chains for each RCP is shown in brackets.

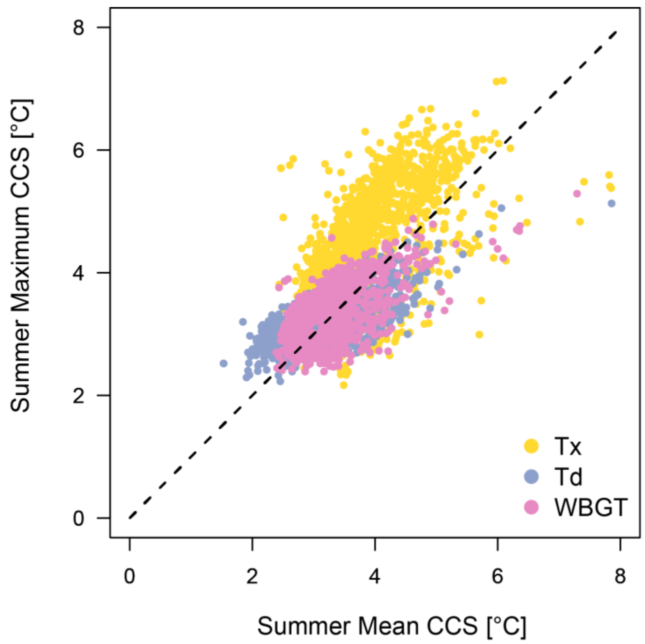

Figure S7 Amplification of the climate change signal in temperature extremes. Station-based mean vs. maximum multi-model median climate change signal (CCS, in °C) in summer for RCP8.5 for daily maximum temperature (T_x), dew point temperature (T_d) and heat exposure in the shade (WBGT).

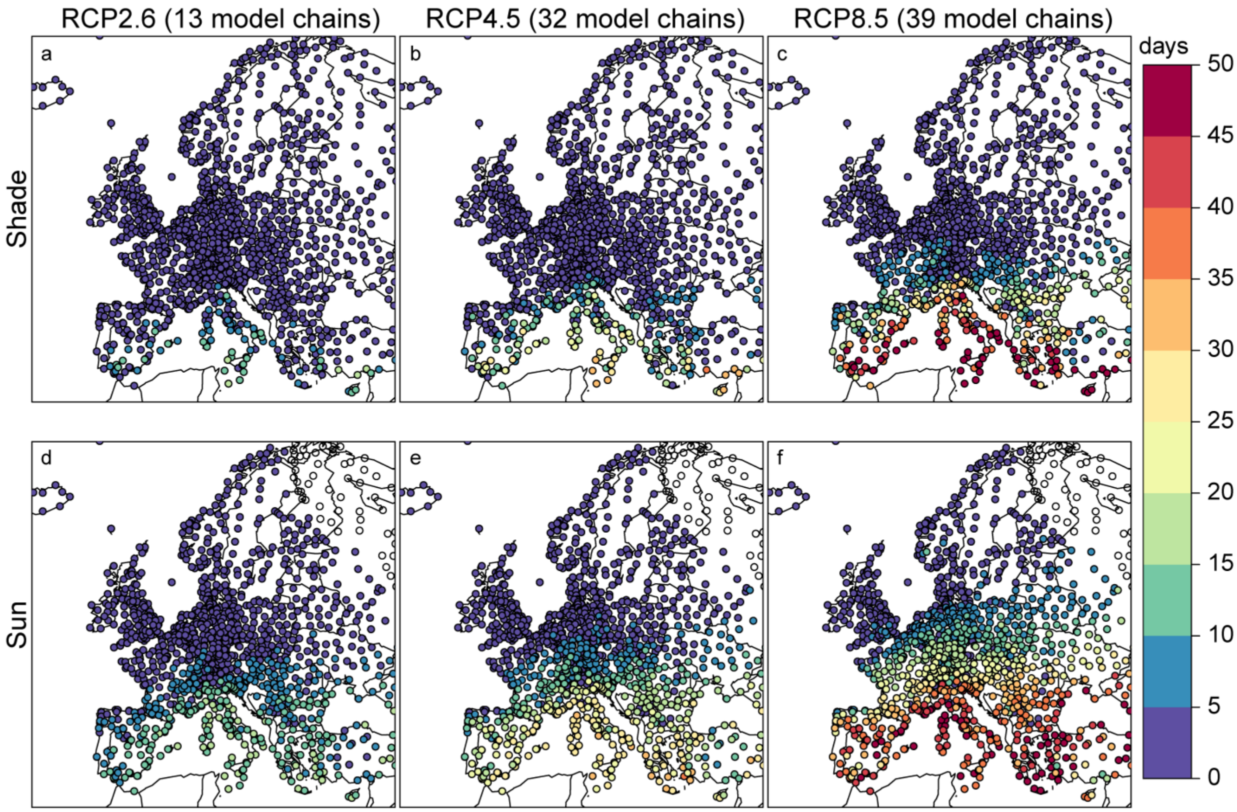

Figure S8 Climate change signal of frequency of high heat risk. As Supplementary Figure S6 but for the number of days with high heat risk (WBGTg28).

References

Addor, N., Rohrer, M., Furrer, R. and Seibert, J. (2016) Propagation of biases in climate models from the synoptic to the regional scale: Implications for bias adjustment. *Journal of Geophysical Research: Atmospheres,* 121, pp. 2075-2089.

Casanueva, A., J. Bedia, S. Herrera, J. Fernández and J. M. Gutiérrez (2018) Direct and component-wise bias correction of multi-variate climate indices: the percentile adjustment function diagnostic tool. *Climatic Change,* 147, pp. 411-425.

Ehret, U., E. Zehe, V. Wulfmeyer, K. Warrach-Sagi and J. Liebert (2012) HESS Opinions ``Should we apply bias correction to global and regional climate model data?". *Hydrol. Earth Syst. Sci.*, 9, 16, pp. 3391-3404.

Fischer, E. M., Oleson, K. W. and Lawrence, D. M. (2012) Contrasting urban and rural heat stress responses to climate change. *Geophysical Research Letters,* 39.

Gobiet, A., Suklitsch, M. and Heinrich, G. (2015) The effect of empirical-statistical correction of intensity-dependent model errors on the temperature climate change signal. *Hydrology and Earth System Sciences,* 19, pp. 4055-4066.

Gudmundsson, L., Bremnes, J. B., Haugen, J. E. and Engen-Skaugen, T. (2012) Technical Note: Downscaling RCM precipitation to the station scale using statistical transformations; a comparison of methods. *Hydrology and Earth System Sciences,* 16, pp. 3383-3390.

Gutiérrez, J. M., D. Maraun, M. Widmann, R. Huth, E. Hertig, R. Benestad, O. Roessler, J. Wibig, R. Wilcke, S. Kotlarski, D. San Martín, S. Herrera, J. Bedia, A. Casanueva, R. Manzanas, M. Iturbide, M. Vrac, M. Dubrovsky, J. Ribalaygua, J. Pórtoles, O. Räty, J. Räisänen, B. Hingray, D. Raynaud, M. J. Casado, P. Ramos, T. Zerenner, M. Turco, T. Bosshard, P. Štěpánek, J. Bartholy, R. Pongracz, D. E. Keller, A. M. Fischer, R. M. Cardoso, P. M. M. Soares, B. Czernecki and C. Pagé (2018) An intercomparison of a large ensemble of statistical downscaling methods over Europe: Results from the VALUE perfect predictor cross-validation experiment. *International Journal of Climatology*.

Havenith, G. and Fiala, D. (2015) Thermal Indices and Thermophysiological Modeling for Heat Stress. En: *Comprehensive Physiology.* American Cancer Society, pp. 255-302.

Hertig, E., D. Maraun, J. Bartholy, R. Pongracz, M. Vrac, I. Mares, J. M. Gutiérrez, J. Wibig, A. Casanueva and P. M. M. Soares (2018) Comparison of statistical downscaling methods with respect to extreme events over Europe: Validation results from the perfect predictor experiment of the COST Action VALUE. *International Journal of Climatology*.

ISO (1989) *Hot environments - Estimation of the heat stress on working man, based on the WBGT-index (wet bulb globe temperature).* ISO Standard 7243 ed. Geneva: International 371 Standards Organization.

Ivanov, M. A., Luterbacher, J. and Kotlarski, S. (2018) Climate Model Biases and Modification of the Climate Change Signal by Intensity-Dependent Bias Correction. *Journal of Climate*.

Kjellstrom, T., C. Freyberg, B. Lemke, M. Otto and D. Briggs (2018) Estimating population heat exposure and impacts on working people in conjunction with climate change. *International Journal of Biometeorology*, 01 3, 62, pp. 291-306.

Lanzante, J. R., K. W. Dixon, M. J. Nath, C. E. Whitlock and D. Adams-Smith (2018) Some Pitfalls in Statistical Downscaling of Future Climate. *Bulletin of the American Meteorological Society*, 99, pp. 791-803.

Maraun, D. (2013) Bias Correction, Quantile Mapping, and Downscaling: Revisiting the Inflation Issue. *J. Climate*, 1, 26, pp. 2137-2143.

Maraun, D., T. G. Shepherd, M. Widmann, G. Zappa, D. Walton, J. M. Gutiérrez, S. Hagemann, I. Richter, P. M. M. Soares, A. Hall and L. O. Mearns (2017) Towards process-informed bias correction of climate change simulations. *Nature Climate Change*, 7, pp. 764-773.

Sahu, S., Sett, M. and Kjellstrom, T. (2013) Heat exposure, cardiovascular stress and work productivity in rice harvesters in India: implications for a climate change future.. *Industrial Health*, 51, pp. 424-431.

Vrac, M. and Friederichs, P. (2015) Multivariate—Intervariable, Spatial, and Temporal—Bias Correction. *J. Climate*, 1, 28, pp. 218-237.

Wilcke, R. A. I., Mendlik, T. and Gobiet, A. (2013) Multi-variable error correction of regional climate models. *Climatic Change*, 120, pp. 871-887.

Wyndham, C. H. (1969) Adaptation to heat and cold. *Environmental Research*, 2, pp. 442-469.